Science and Technology for Energy Transition **78**, 7 (2023)

https://doi.org/10.2516/stet/2023001

Available online at:
stet-review.org

REGULAR ARTICLE OPEN ACCESS

Active power management of grid-connected PV-PEV using a Hybrid GRFO-ITSA technique

Chagam Reddy Subba Rami Reddy[1,*], Badathala Venkata Prasanth[2], and Balapanur Mouli Chandra[3]

[1] Department of Electrical and Electronics Engineering, B V Raju Institute of Technology, Vishnupur, Narsapur, Telangana 502313, India
[2] Department of Electrical and Electronics Engineering, Dean Quality Control, Accreditations and Rankings, College of Engineering and Technology, Ongole, Andhra Pradesh 523272, India
[3] Department of Electrical and Electronics Engineering, QIS College of Engineering and Technology, Ongole, Andhra Pradesh 523272, India

Received: 19 July 2022 / Accepted: 30 January 2023

Abstract. In this manuscript proposed a hybrid *Garra Rufa* Fish Optimization (GRFO) and Improved Tunicate Swarm Algorithm (ITSA) for improving the power quality of the integrated Photovoltaic (PV) and Plug-in Electric Vehicle (PEV) in Smart Grid (SG) system. The GRFO-ITSA approach is hybrid wrapper of GRFO and ITSA. Commonly it is named as GRFO-ITSA approach. The grid-connected PV-PEV, active power management is performed by the proposed approach. The proposed GRFO approach is used to determine the individual harmonic components and to reduce the recompense currents applied to PVs *via* PEV converters. The load flow control is performed by ITSA approach, which controls the power among the PVs, and PEVs. Additionally, it satisfies the power demand, and voltage variation. The proposed approach is also to analyze the mutual properties of PVs as well as PEVs on the feeder and transmitting loads, voltage outlines, harmonic alterations of an urban electric power distribution system. Also, the performance of the GRFO-ITSA is implemented on MATLAB site as well as associated with several existing approaches. The GRFO-ITSA have improved the power quality and compensate the harmonics and reactive power of the system. The optimal outcome is obtained by GRFO-ITSA with less computation time.

Keywords: Photovoltaic (PV), Plug-in Electric Vehicle (PEV), Smart Grid (SG), Load flow control, Harmonics reduction, Electric power distribution system.

1 Introduction

In the present days the distribution of power systems is very big as well as some difficulties are present in the system [1]. Furthermore, due to the growth of nonlinear loads and number of customers, the production of power become more and more hassled [2]. The proper functioning of the utility and consumer devices is damaged by the presence of electrical pollution and frequency distortion because of nonlinear loads and high customers [3]. Renewable Energy Resources (RESs) have been employed at the utility stage to enable future power systems operate at peak efficiency and to alleviate environmental troubles [4]. The removal of the hazardous emissions and increasing the utilization of renewable sources are the main merits of the renewable power generation [5]. PV is the main source of RESs and the output capacity of PV is increasing at low voltage, which provides difficulties in the system operator [6]. Clouds induce small variation in PV output [7].

The quality of power is affected by the intermittent nature of PV generation. Voltage variations along light spark triggered through voltage variations are major power quality issues connected to fast PV output variations [8]. Damage is occurring to electric devices linked to the network by the voltage fluctuations and flickers [9] as well as health problems are occurring based on the light flicker. There are various researches are carried the relation among PV power output fluctuations and light flicker [10]. Thus reduce the issue of the power quality induced by the PV outcome fluctuation needs the advanced approaches [11]. The voltage fluctuations are not mitigated by using the On-Load Tap Changers (OLTCs) at transmit stations [12]. Scrapyard loads as well as diesel generators combined utilize battery systems is unwanted to mitigate PV fluctuations because scrapyard loads dissipate solar energy along diesel generators has negative environment powers

* Corresponding author: csubbaramireddy2020@gmail.com

[13]. Reactive control in PV inverters is reducing PV power generation fluctuations, which affect the inverter [14]. Moreover, the voltage drop of the PV system is minimized by the combination of Maximum Power Point Tracking (MPPT) approach and DC-DC converter [15].

In recent times, Electric Vehicle (EV) batteries are more suited for a gorgeous technology for minimizing the fluctuations [16]. In the future, the adaptation of EV should increase, so charging EV is done with high count of EV batteries are associated to grid [17]. The investment of system operator as well as social cost is reduced through the portion of the battery capacity is used for grid services by accumulators that attach a set of EVs [18]. There are various approaches are utilized to enhance the power quality. One of the approaches is present harmonic control method, which is functional in solitary-phase inverters for solar system [19]. The harmonic components are detected by the usage of dropped synchronization phase-locked loops and compensation is done through the proportional resonant current regulator [20].

In this manuscript proposed a hybrid GRFO-ITSA approach for improving the power quality of the integrated PV and PEV in SG system. The GRFO-ITSA control approach is the hybrid wrapper of Garra Rufa Fish Optimization (GRFO) and improved Tunicate Swarm Algorithm (ITSA). Commonly it is named as GRFO-ITSA approach. The grid-connected PV-PEV, active power management is performed by the proposed approach. The recreation of the manuscript is labelled as below: Section 2 illuminates bibliographic survey and its contextual. Section 3 describes the configuration of the integrated PV, PEV system in SG for power quality improvement. Section 4 describes the method of controlling PEV using phase-linked photovoltaics and the proposed approach. Section 5 illuminates the proposed approach based power quality improvement; Section 6 is the result along discussion. Section 7 concludes the manuscript.

2 Recent research works: a briefly appraisal

Many research projects based on the integration of photovoltaic generators use PEVs in electric SG using a variety of methods and features. Some of them are reviewed here.

Balasundar *et al.* [21] has Adaptive Neuro-Fusi Restricted Distribution standard compensation was recommended to improve the quality of the distribution grid EV Charging Station (CS). The EVCS was powered by a 3-phase duplex AC-DC converter, duplex helicopter, distributive static compensator and lithium-ion battery. The flow of power from grid to vehicle before vehicle to grid was assisted by bidirectional converters. The bidirectional chopper was controlled by multi-step current control approach. Gayathri [22] have elucidated vehicle electrification from smart grid concept. The information about the electric vehicle and EV functioning were evaluated the components of EV. The research was analyzed the Electric drives, battery, renewable ES, charging approaches, ESS and power management, optimization approaches. Brinkel *et al.* [23] have suggested the alleviation of PV output changeability through shifting the charging processes of Electric Vehicles (EVs). The introduced model was determining the effect of variation of PV output on the power quality of grid at low voltage grid. The variation of output power of PV was performed by the analysis of load flow.

Lara *et al.* [24] have suggested the Single-Phase (SP) Active-Neutral Point Clamped (ANPC) Five-Level Bidirectional Converter (FLBC) for increasing the power quality. The quality of power was improved by the connection of G2V and V2G operation performed and connected in series manner. By utilizing the Dual-Active Half-Bridge DC-DC Converter (DAHBC) utilize a huge frequency isolation transmitter, the EV charger operation was performed. The introduced model was utilized ten numbers of switches. The introduced converter was reduces the stress of switching devices, minimize the losses of the system. Irfan *et al.* [25] have suggested neuro-fuzzy control approach in reduction for harmonics. The introduced method was utilized the shunt active power filter. Kavin and Subha Karuvelam [26] have elucidated the SEPIC converter for solar panel and grid utilizes the electrical vehicle system. The introduced converter was operate at low duty cycle and provides high dc voltage, less switching loss. Based on BLDC motor-fed electric train along grid *via* a 3-phase and SP inverters, the introduced converter outcome was obtained. PI controller was utilized to control the converter. The daytime produced power of solar was applied to the EV and grid and by utilizing the converter in nightly period, the power was supply as of grid to EV. Bajaj and Singh [27] have introduced Analytic Hierarchy Process (AHP) for evaluation of quality power. Evaluation of quality power was provides centralized Global Power Quality Index (GPQI). The introduced system was incorporated with the utility, load, and DG.

2.1 Contextual of the research work

The review of the current research works depicts that the managing of grid-connected PV and plug-in electric vehicle is the most challenging task. Recently, improving the quality of power used in intelligent network power has been considered a key challenge in the successful smart grid. Due to the increase in solar PVs and EVs the power grid experiences high intermittency as well as uncertainty on the production and demand sides, which can place high loads on the distributing network and disturb the steadiness and grid power quality. Though, the combined function of solar PV and EV charging complements each other. Because of the individual combination of PV and EVCS, it deals with issues such as grid stability and quality electricity. Furthermore, mass spreads, PVs and EVs have been used to create new participants in the energy market process, as well as play a key role in redefining the market. The evaluation of individual effect of EV charge along photovoltaic system on the operational grid has investigated recently in various research works. But, the integration of effects of PVs and EVs on stability of grid, power quality as well as energy economics have evaluated in only very few research works. Hence advanced approaches are needed to analyze the effects of combined process of PV and EV. These disadvantages were encourage to do this research work.

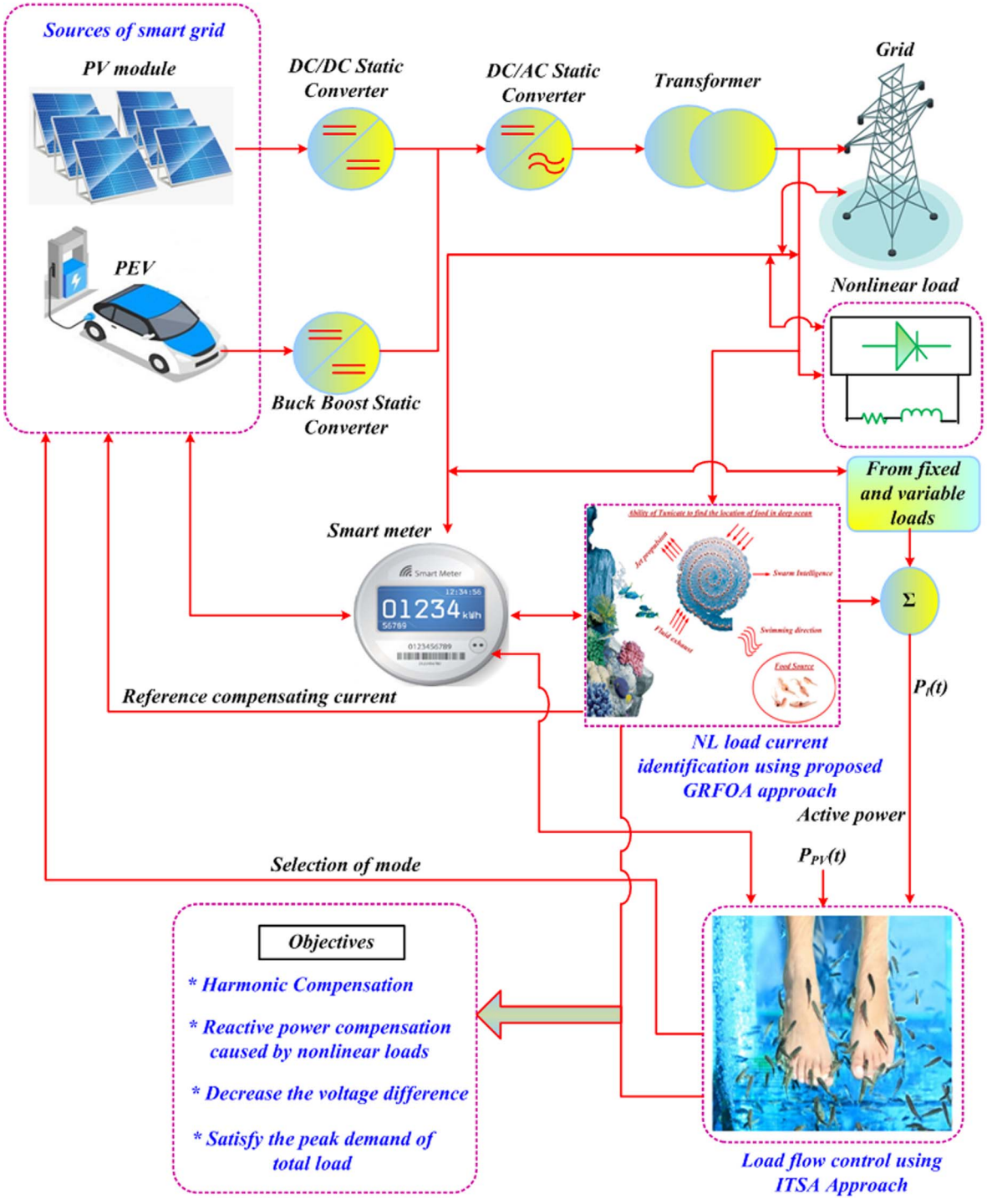

Figure 1. Configuration of integrated PV and PEV system with proposed approach.

3 Configuration of integrating photovoltaic and PEV in SG for power quality enhancement

Figure 1 depicts the configuration of integrating photovoltaic as well as PEV system in SG with proposed approach. Here, PEVs are operating both the grid to vehicle (G2V), vehicle to grid (V2G) mode. In the V2G mode PEV act as power generators and in G2V mode, it act as consumer load. To obtain the maximal power point generation along control of dc connection power, at every PV source terminal is utilized the boost DC/DC static converter. Similarly, to control the DC link voltage of PEV and to enable the power flow of each PEV during the charging or discharging process, PEV is connected to the buck boost

static converter. To regulate the flow of power assigned to deliver load as well as to participate in ancillary services, each unit of PVs and PEVs is associated to SG by the DC/AC static converter. The loads such as nonlinear load, fixed load and adjustable loads are connected to the system [28]. Harmonics are formed due to the utilization of nonlinear load. So to alleviate the harmonics of the system, in this paper proposed a hybrid GRFO-ITSA approach. The major objectives of the proposed approach are compensation of harmonics, compensation of reactive power caused by nonlinear loads, control of grid frequency, and satisfaction of load demand. In the proposed system utilized the smart meter for the purpose of data collection, information sending as well as receive the instructed information. So the smart meter is connected to all the components of the system like PV, PEV, load, etc.

The smart meter collects the information like current and voltage of the nonlinear loads, daily requirement of the load, generation of PV power, preferred constraints of active powers, battery capacity of PEVs as well as its connection and disconnection time at CS. The collected information is received by the proposed hybrid approach. The proposed approach is operated under two sections such as neuronal nonlinear loads currents identification using GRFO approach. The proposed GRFO approach input is current and voltage of the nonlinear loads. The outcome becomes reference compensating currents. To guarantee the harmonic and reactive current mitigation, these reference compensating currents is given to the inverter of PEVs and PVs. This approach also provides the nonlinear loads active power which is given to the grid disturbance control using ITSA approach. The input phase of ITSA approaches are connecting loads; *i.e.* nearby information that PVs generate electricity and connect PEVs. Then, it controls the flow of power transmitted between the loaders to achieve a continuous load distribution and maintains the stability of the system. Consider an urban area Electric power Distribution System (EDS) which is incorporated with feeders, transformers; lumped loads represent industrial, commercial and residential loads. Consider three numbers of transformers like t_{r1}, t_{r2}, t_{r3} which feed the loads of industrial, commercial and residential.

3.1 Photovoltaic (PV) model

In PV system the electrical energy is obtained from the operation of solar cell. The extracted PV power is expressed by using equation (1),

$$P_{\mathrm{PV}} = P_{\mathrm{STD}} \frac{G_{\mathrm{ir}}}{G_{\mathrm{STD}}} (1 + k(T_{\mathrm{c}} - T_{\mathrm{ref}})), \tag{1}$$

here power at standard condition is denoted as P_{STD}, incident irradiance is denoted as G_{ir}, irradiance at standard condition is denoted as G_{STD}, temperature coefficient of power is denoted as k, cell temperature implies T_{c}, reference temperature implies T_{ref}. PV power used in the load requirement and that can reversely inject to the grid which is described as,

$$P_T^{\mathrm{PV}} = P_T^{\mathrm{PV}_k} + P_T^{\mathrm{PV}_s}, \quad \forall T \tag{2}$$

here power injected to grid from the PV is denoted as $P_T^{\mathrm{PV}_k}$, power used to satisfy load from the PV (kW) is denoted as $P_T^{\mathrm{PV}_s}$.

For the penetration levels of PVs, fitting power percentage about fitting power of the transmitter is described by,

$$\mathrm{PVs}\,(\%) = \frac{A_{\mathrm{PVs}}}{A_{\mathrm{Trans}}} \times 100\% \tag{3}$$

here overall fitting seeming power of PVs in the perceived transmitting place is denoted as A_{PVs}, fitting seeming power of the transmitter in the perceived transmitting place is denoted as A_{Trans}.

3.2 Electric vehicle model

In addition to absorbing energy, PEVs are used to provide great quality support in the power network, and are an integral part of the Smart Grid [29]. Commonly PEVs are incorporated with battery and the charging station. The most challenge of the PEV is efficiency of the battery. The proposed system is utilized the Lithium battery packets connected utilize a duplex DC/AC converter. Notice that the battery is based on the voltage connected in series with the resistor. Based on the direction of current, recognized the charging and discharging operation of battery. The discharging process is turn on if the battery current is positive and the charge process is turn on if the battery current is negative. The charging and discharge process is described as,

$$V_{\mathrm{Bat}} = u_o - ri - k\frac{q}{i \cdot t - 0.1q} i^* - k\frac{q}{q - i \cdot t} i \cdot t + Ae^{-b \cdot i \cdot t} \tag{4}$$

$$V_{\mathrm{Bat}} = u_o - ri - k\frac{q}{q - i \cdot t} i^* - r\frac{q}{q - i \cdot t} i \cdot t + Ae^{-b \cdot i \cdot t} \tag{5}$$

To obtain the configuration of battery pack, the Li-ion batteries are associated in sequence and similar manner, which is utilized for achieving net voltage as well as current requirement. The State of Charge (SOC) of the battery is described as,

$$\mathrm{SOC} = 100\left(1 - \frac{i \cdot t}{q}\right). \tag{6}$$

The charging and discharging limit is described by,

$$P_{\mathrm{Min}} \le P_{\mathrm{ev}} \le P_{\mathrm{Max}}. \tag{7}$$

The limit of the SOC is described as,

$$\mathrm{SOC}_{\mathrm{Min}} \le \mathrm{SOC} \le \mathrm{SOC}_{\mathrm{Max}}. \tag{8}$$

The travelling power is described depend on the distance which is espressed as,

$$p_{\mathrm{tr}} = \mu_{\mathrm{pev}} \cdot ad. \tag{9}$$

For the penetration levels of PVs, fitting power percentage about fitting power of the transmitter is described by,

$$\text{PEVs}\,(\%) = \frac{A_{\text{PEVs}}}{A_{\text{Trans}}} \times 100\%, \tag{10}$$

here overall fitting seeming power of PEVs in the perceiving transmitter place is denoted as A_{PEVs}, fitting seeming power of the transmitter in the perceiving transmitter place is denoted as A_{Trans}.

3.3 DC-DC converter model

The dc bus voltage is obtained by the DC-DC converter [30]. The duty cycle of the converter is described by,

$$\text{dc} = 1 - \left(\frac{V_{\text{i}}}{V_{\text{o}}}\right), \tag{11}$$

here input voltage is denoted as V_{i}, output voltage is denoted as V_{o}.

3.4 Voltage along current harmonic distortion

An active nonlinear devices are present in the system which producing the harmonics. To determine the performance of the system must determine the total voltage harmonic distortion and total current harmonic distortion [31]. The relation of the sum of the power of all harmonic current instruments with the power of the essential current frequency is called the total current harmonic decay, which is described by,

$$\text{TVHD} = \frac{100 \times \sqrt{v_{\text{rms}}^2 - v_{\text{frms}}^2}}{v_{\text{frms}}}, \tag{12}$$

$$\text{TIHD} = \frac{100 \times \sqrt{i_{\text{rms}}^2 - i_{\text{frms}}^2}}{i_{\text{frms}}}, \tag{13}$$

here TVHD denotes overall voltage harmonic distortion, TIHD denotes overall current harmonic distortion, v_{frms} denotes fundamental voltage frequency, i_{frms} denotes fundamental current frequency, v_{rms} denotes harmonic voltage component, i_{rms} denotes harmonic current component.

4 Control approach of proposed system

To solve the power quality problems, the proposed GRFO-ITSA approach is utilized in the combined PVs and PEVs connected to SG system. The first part of the proposed approach is neuronal nonlinear load current identification using GRFO approach which can reduce the harmonics by using the reference current generation of the system.

4.1 Nonlinear load current identification system

To mitigate the harmonics and compensate the reactive power utilized the non linear load current identification. By utilizing the proposed GRFO approach, reference current is applied to PV, PEV unit, then the determinations of each individual harmonics are achieved. Figure 2

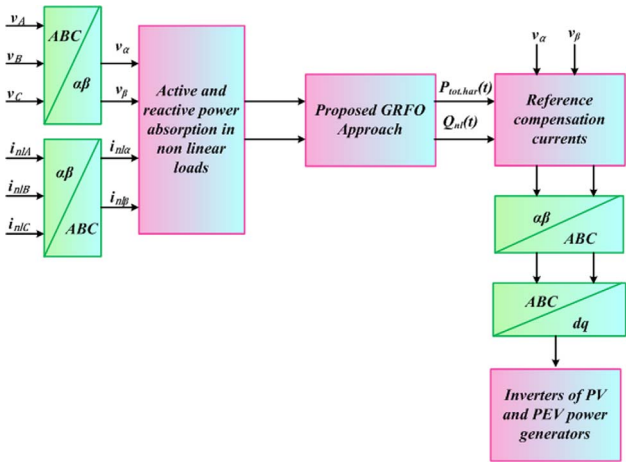

Figure 2. Control structure of the proposed GRFO approach.

shows that the Control structure of the proposed GRFO approach. The voltage is described as the point of the joint coupler 1,

$$\begin{bmatrix} \boldsymbol{V_A} = \sqrt{\boldsymbol{2}}\,\boldsymbol{V}\sin(\boldsymbol{\omega T}) \\ \boldsymbol{V_B} = \sqrt{\boldsymbol{2}}\,\boldsymbol{V}\sin\left(\boldsymbol{\omega T} - \dfrac{\boldsymbol{2\pi}}{\boldsymbol{3}}\right) \\ \boldsymbol{V_C} = \sqrt{\boldsymbol{2}}\,\boldsymbol{V}\sin\left(\boldsymbol{\omega T} + \dfrac{\boldsymbol{2\pi}}{\boldsymbol{3}}\right) \end{bmatrix}. \tag{14}$$

The nonlinear load is parallel to the rl load, which produce the harmonics to the grid which is described as follows,

$$\begin{bmatrix} \boldsymbol{i_{hA}} \\ \boldsymbol{i_{hB}} \\ \boldsymbol{i_{hC}} \end{bmatrix} = \sqrt{\boldsymbol{2}\boldsymbol{i_1}} \begin{bmatrix} \displaystyle\sum_{N=1,5,7,11,13} \frac{\boldsymbol{1}}{\boldsymbol{N}} \sin(\boldsymbol{N}(\boldsymbol{\omega T} - \boldsymbol{\phi})) \\ \displaystyle\sum_{N=1,5,7,11,13} \frac{\boldsymbol{1}}{\boldsymbol{N}} \sin\left(\boldsymbol{N}\left(\boldsymbol{\omega T} - \boldsymbol{\phi} - \frac{\boldsymbol{2\pi}}{\boldsymbol{3}}\right)\right) \\ \displaystyle\sum_{N=1,5,7,11,13} \frac{\boldsymbol{1}}{\boldsymbol{N}} \sin\left(\boldsymbol{N}\left(\boldsymbol{\omega T} - \boldsymbol{\phi} + \frac{\boldsymbol{2\pi}}{\boldsymbol{3}}\right)\right) \end{bmatrix}, \tag{15}$$

here the fundamental frequency is denoted as ω, phase angle among the current and load voltage is denoted as ϕ. Based on the orthogonal coordinates the nonlinear load current as well as voltage is described as,

$$\begin{bmatrix} \boldsymbol{i_{nl_\alpha}} \\ \boldsymbol{i_{nl_\beta}} \end{bmatrix} = \sqrt{\boldsymbol{3}\boldsymbol{i_1}} \begin{bmatrix} \displaystyle\sum_{N=1,5,7,11,13} \frac{\boldsymbol{1}}{\boldsymbol{N}} \sin(\boldsymbol{N}(\boldsymbol{\omega T} - \boldsymbol{\phi})) \\ \pm \displaystyle\sum_{N=1,5,7,11,13} \frac{\boldsymbol{1}}{\boldsymbol{N}} \cos(\boldsymbol{N}(\boldsymbol{\omega T} - \boldsymbol{\phi})) \end{bmatrix}, \tag{16}$$

$$\begin{bmatrix} \boldsymbol{v_\alpha} \\ \boldsymbol{v_\beta} \end{bmatrix} = \sqrt{\boldsymbol{3}\boldsymbol{v_s}} \begin{bmatrix} \sin(\boldsymbol{\omega T}) \\ -\cos(\boldsymbol{\omega T}) \end{bmatrix}. \tag{17}$$

The active and reactive power based on the nonlinear load is described as,

$$\begin{bmatrix} \boldsymbol{P_{nl}} \\ \boldsymbol{Q_{nl}} \end{bmatrix} = \begin{bmatrix} \boldsymbol{v_\alpha i_{nl_\alpha}} + \boldsymbol{v_\beta i_{nl_\beta}} \\ \boldsymbol{v_\alpha i_{nl_\beta}} + \boldsymbol{v_\beta i_{nl_\alpha}} \end{bmatrix}, \tag{18}$$

here the error is calculated by,

$$E = P_{nl}(t) - P_{nl,\mathrm{Est}}(t), \tag{19}$$

here the instantaneous power is denoted as $P_{nl}(t)$, estimated active power is denoted as $P_{nl,\mathrm{Est}}(t)$. The harmonic power is eliminated by the compensation of difference among the fundamental active power, instantaneous active power.

The harmonic of the reference current and reactive power compensation is achieved by the determination of net harmonic power which is described as follows,

$$\begin{bmatrix} i_{\mathrm{cpen-Ref}-\alpha} \\ i_{\mathrm{cpen-Ref}-\beta} \end{bmatrix} = \frac{1}{v_\alpha^2 + v_\beta^2} \begin{bmatrix} v_\alpha & -v_\beta \\ v_\beta & v_\alpha \end{bmatrix} \cdot \begin{bmatrix} P_{\mathrm{tot.har}} \\ Q_{nl} \end{bmatrix}. \tag{20}$$

The reference currents are compensated then it is classified into PV and PEV inverters. When no PV is connected to the CS then the harmonics and the reactive power is recompensed through PV generators [32–35]. If the PEV is connected to the PV then it share the reference currents and compensate both the reactive power and harmonics. In PV inverter, the reference current compensation in the dq axis is described as,

$$i_{\mathrm{PV}k-\mathrm{cpen-Ref}-d} = \left(i_{\mathrm{cpen-Ref}-d} - \sum_{1}^{N} i_{\mathrm{PV}j-\mathrm{cpen-Ref}-d} \right) N_{\mathrm{PV}}, \tag{21}$$

$$i_{\mathrm{PV}k-\mathrm{cpen-Ref}-q} = \left(i_{\mathrm{cpen-Ref}-q} - \sum_{1}^{N} i_{\mathrm{PEV}j-\mathrm{cpen-Ref}-q} \right) N_{\mathrm{PV}}. \tag{22}$$

4.2 Load flow control

If the smart grid is incorporated with variable load demands then the active power production as well as consumption provides the imbalance of power. So the control of load flow balanced by the proposed ITSA approach [36]. Here, the lumped loads, PVs generation, plug in as well as plug out time of PEV, SOV of battery are considered. The measurement of the quantities of the electrical power distributing system voltage harmonics for the grid and lumped load current harmonics is determined. The harmonic load flow control is performed by the ITSA approach. Here considered the odd harmonics for example 3rd, 5th, 7th, 9th, 11th, 13th harmonics. In first and last order harmonics utilized by the 10 kV MV grid.

5 Proposed GRFO-ITSA approach based power quality improvement in the simultaneous integration of PVS and PEV system

In this study a hybrid GRFO-ITSA is proposed the power value and to analyze day-to-day load details in the feeders along transmitters as well as effect of simultaneous integration of PVS and PEV [37–39] on the daily voltage and total harmonic distortion of voltage profiles in the urban electric power distribution system. Using the proposed approach, modeled the connection and disconnection of PEV in CS and the loads. The harmonic distortion is minimized by the proposed GRFO-ITSA approach. The detailed description of the proposed approach is described as below.

5.1 Reference current generation using Garra Rufa Fish Optimization algorithm (GRFO)

GRFO is the new Optimization approach which is stimulated through spectacular movements of the Garra Rufa fish among two legs sunk through an usual "fish rubbing assembly". In this GRFO, the particles are splitted into group and the best one is found in each group [40]. Based on the fitness of the group leader, some of these particles are permitted to adjust groups. The mobility between the groups is obtained by the number of fishes present in each group. The fishes are present in different groups when searching their food and each group has an own way to found the operating point of the system. Each group incorporated with leader and identical number of particles which is known as follower. Based on the value the follower changes their groups for all iteration. In this manuscript, GRFO is utilizes to calculate reference current in an integrated PV-PEV system. Gradually process of GRFO described in below:

Step 1: Initialization

In this initialization step, the currents and voltage values, and load demand are initialized.

Step 2: Random generation

An initialized parameters are arbitrarily generated in the form of matrix.

Step 3: Fitness calculation

Fitness calculation is found depend on the objective of the system. It is described as,

$$F_i = \mathrm{Min}(e), \tag{23}$$

here e is the error function.

Depending on fitness function, restore the system parameters.

Step 4: Resort the parameter

Based on the fitness function, resort the parameter of the system.

Step 5: Check the iteration

Check the maximum iteration, if obtained the maximum iteration then obtain the optimal reference value.

The numbers of leaders are used to select to allow for the difficulty of the problems and the expect number contains the optimal points for the objective process. Each time a particular group of fish travels towards an additional group, it is best to pay the optimal fare between the whole group. If not attain the maximum iteration then go to next step.

Step 6: Update the parameter

Update the number of particles for each group is described by,

$$N_f = \frac{n - N_L}{N_L}, \tag{24}$$

here total number of particles is denoted as n, number of followers represent N_f, number of leaders indicates N_L.

Step 7: Find worst and best leader

The worst leader is described as,

$$N_f = \text{int}(\alpha \times \text{rand}), \tag{25}$$

$$m_{ij} = \max\left(\left(m_{ij-1} - N_f\right), 0\right), \tag{26}$$

here, Mobile fish for ith leader is denoted as M_{ij}. The best leader is determined by,

$$N_1 = \sum_{2}^{n} N_i, \tag{27}$$

$$m_{1j} = m_{1,j-1} + N_1. \tag{28}$$

Step 8: Update the position and speed

The position and velocity is determined by the below equations,

$$v_i(t+1) = \omega v_i(t) + c_1 R_1(p_i(t) - X_i(t)) + c_2 R_2(g_i(t) - X_i(t)), \tag{29}$$

$$X_i(t+1) = X_i(t) + v_i(t+1), \tag{30}$$

here speed of the ith atom is denoted as V_i, inactivity mass parameter is denoted as ω, acceleration coefficients is denoted as C_1, C_2. After updation, the loop is connected to step 3.

5.2 ITSA for load demand satisfaction

TSA is one of the bio-inspired metamorphic optimizing algorithms. In the swarming activity of the Mytilus, this mechanism encourages them to survive efficiently in the complex conditions of the ocean [41–44]. To determine the location of food source in sea Tunicate has a great talent. There are two characteristic of tunicates like jet momentum as well as swarm performances are used for searching the food source of the sea. Based on these two characteristic tunicate determine the optimum food source. In this paper the TSA is improved by the cross over and mutation operator hence, named as improved TSA approach. ITSA is used to satisfy the load demand of the system. The step by step process is described as below [45–47].

Step 1: Initialization

TSA input vectors operate from the GRFO approach, load demand that is initialized in the initialization.

Step 2: Random generation

Spontaneous function is used to generate numbers in the middle of [0, 1]. Based on the problem area, the lesser limit was chosen with the higher limit.

Step 3: Fitness Assessment

Determines the fitness of every searching agent. The assessment of fitness is determined as the objective function. It is regulated as,

$$\text{Obj} = \text{Min}\,(\text{voltage deviation, harmonics}) \tag{31}$$

Step 4: Position Upgrading

Determine the jet velocity and mass behaviour of the Mytilus based on fitness and upgrade location using the equation below,

$$t_p = \left(\frac{\rho}{y} + 1\right) = \frac{\bar{t}_p(y) + t_p\left(\frac{\rho}{y} + 1\right)}{2 + o_1}, \tag{32}$$

here $\bar{t}_p(y)$ is the position of tunicate, o_1 is the random number.

Step 5: Crossover along mutation:

The upgrade function uses the shortcut with the mutation operator by rearranging the Mytilus swarm location. In two individuals to create a newly solution package, the shortcut ratio is achieved.

$$X_{\text{over}} = \frac{\delta}{\kappa}, \tag{33}$$

here δ implies count of individuals crossover, κ implies distance of individuals.

Individuals are approximately transmitted in light of the exact ratio of change in the process of change

$$Y_{mu} = \frac{\pi}{\mu} \tag{34}$$

here π indicates transmit point, L indicates distance of individuals.

Step 6: Boundary analysis

Check whether the renewal search agent location is within or outside the boundaries.

Step 7: Computing fitness

Determines the improved status of the Mytilus fitness function using error function resolution

Step 8: Termination

Once the conclusion principles are fulfilled rather than the optimal solution for the search, go to Step 4. Figure 3 illustrates the flow chart of the GRFO-ITSA approach.

6 Results and discussion

This manuscript describes the performance of the proposed GRFO-ITSA. In this manuscript proposed GRFO-ITSA for improving the quality of power. The photovoltaic as well as PEV are concurrently connected together in SG system. The active power is managed by GRFO approach and load is controlled by the ITSA approach. The major aim of GRFO-ITSA is minimizes the deviation of voltage, total harmonic distortion minimization. The proposed approach is to analyze the mutual properties of the PVSs in the PEVs in the feeder, as well as the transmitting load, voltage outlines, and compatible modifications of the city power supply system. Also, the performance of the GRFO-ITSA is implemented on MATLAB site along compared with various existing approaches. Based on two seasons like summer and winter the performance of the system is analyzed.

Figure 4 displays the test system which incorporated with medium and low voltage grid, feeders, distribution transformer stations, and lumped loads expressed as industrial, commercial and residential loads. The design of total loads will be based on the electrical measurement data for summer and winter, especially the three specific summers (June, July and August) and winter (December, January and February).The mean and standard deviation of the load profile is determined from at every 10 min interval.

Case 1: Performance analysis of GRFO-ITSA system on summer

Here, the performance of the GRFO-ITSA is analyzed in summer season. Figure 5 displays the statistical parameters of active energy profiles of lumped loads for summer. Here present the industrial, commercial, residential load mean and standard deviation. The standard deviation of commercial load active power is varies 0 to 0.1(p.u) at the time period of 0 to 24 h. Similarly, the standard deviation of industrial load is varies 0 to 0.15 at the time period of 0 to 24 h. The standard deviation of residential load is varies 0 to 0.18 at the time period 1 h, then it varies from 0.01 to 0.1 (p.u) at 2 to 16 h. After that it varies up to 0.1 0.4 (p.u) at 16 to 24 h respectively. By comparing the mean value of manufacturing profitable along domestic load active powers, the commercial load active power is high then other two active powers. The active power values are normalized about maximal active load power. Analysis of daily profile of the feeder 1 to 2 loads (any type) through summer is displays in Figure 6. Here, the proposed system is analyzed under four sub cases. S base means the system performance is analyzed at PV system and PEVs are not connected in summer (S). S PVS3 means the system is connected to PV system but not connected to the PEV. S PEV3 means the system is connected to PEV but not connected to the PVs. S PVS3 plus PEV3 means the system is connected to both PVs and PEV. For analyzing the time period of 6–18 h, the apparent power at base case is varied up to 850 kVA. Under the connection of PV system, the apparent power is varied up to 500 kVA. By connecting the PV system, the apparent power is very low. When only connecting the PEV, then the apparent power is varied up to 1100 kVA. It provides high apparent power. When connecting both PEV and PV, the apparent power is varied to 650 kVA. It is higher than the connection of individual PV system. Analysis of daily profiles of industrial load at the transformer 1 during summer is displays in Figure 7. Consider the time period 6 to 16 h. At the base case, the apparent power (total power) becomes varied up to 950 kVA. When the system is connected in PV only means then the apparent power is varied up to 240 kVA. When the system is connected in PEV only means then the apparent power is varied up to 400 kVA. This value is bigger than the PV and PEV connection and only PV connection. When the system is connected in PEV and PV means then the apparent power is varied up to 300 kVA. Analysis of daily profiles of commercial load at the transformer two during summer is displays in Figure 8. Consider the time period 6 to 16 h. At the base case, the apparent power (total power) becomes varied up to 350 kVA. When the system is connected in PV only means then the apparent power is maximally varied up to 225 kVA. When the system is connected in PEV only means then the apparent power is maximally varied up to 375 kVA. This value is bigger than the PV and PEV connection and only PV connection. When the system is connected in PEV and PV means then the apparent power is maximally varied up to 225 kVA. Analysis of daily profiles of residential load at the transformer 3 during summer is displays in Figure 9. Consider the time period 6 to 16 h. At the base case, the apparent power (total power) becomes varied up to 275 kVA. When the system is connected in PV only means then the apparent power is maximally varied up to 140 kVA. When the system is connected in PEV only means then the apparent power is maximally varied up to 175 kVA. When the system is connected in PEV and PV means then the apparent power is maximally varied up to 310 kVA. in the residential type load the maximum apparent power is obtained both the connection of PV and PEV system.

Analysis of system voltage differences in maximum level during summer is shown in Figure 10. Here the nodes and voltage differences are present. The voltage difference of both the connection of PV and PEV system is negative

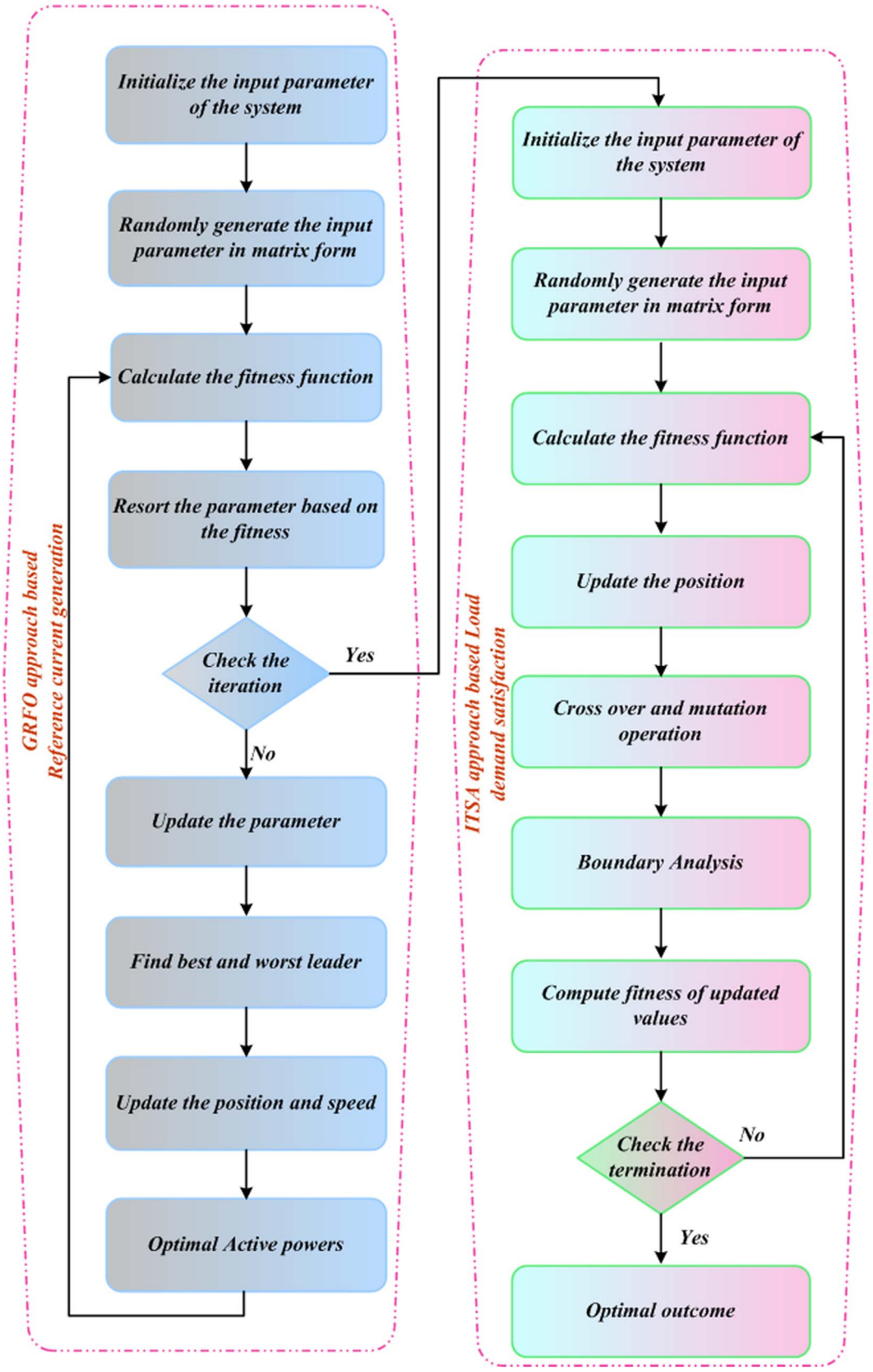

Figure 3. Flowchart of the proposed GRFO-ITSA Approach.

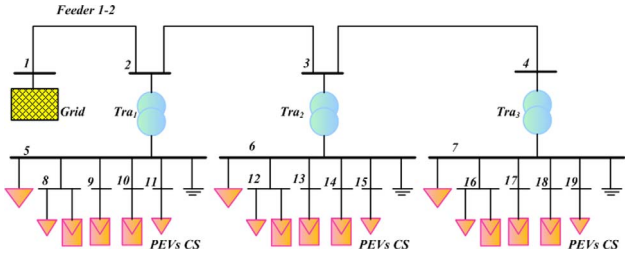

Figure 4. Test system.

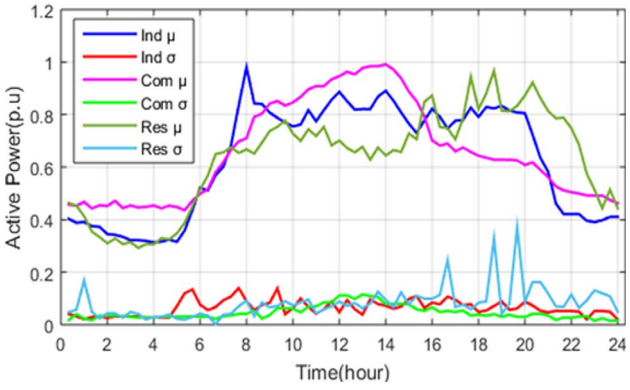

Figure 5. Analysis of statistical parameters of active energy profiles of lumped loads for summertime.

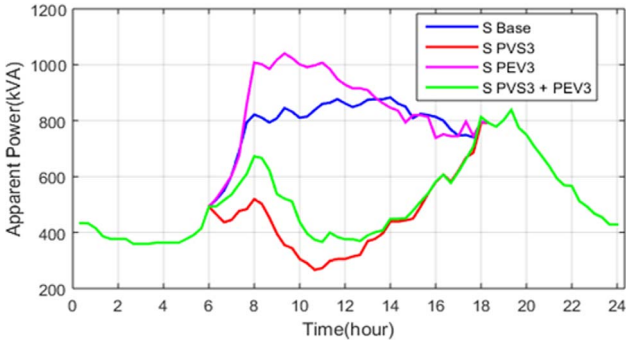

Figure 6. Analysis of day-to-day outlines of the feeder 1 to 2 loads (any type) thru summertime.

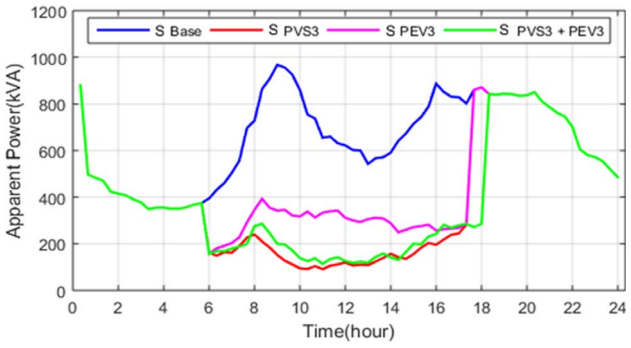

Figure 7. Analysis of day-to-day outlines of manufacturing load at the transmitter 1 thru summertime.

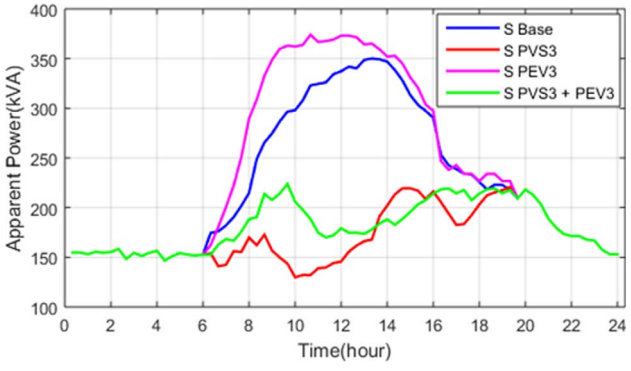

Figure 8. Analysis of day-to-day outlines of profitable load at the transmitter 2 thru summertime.

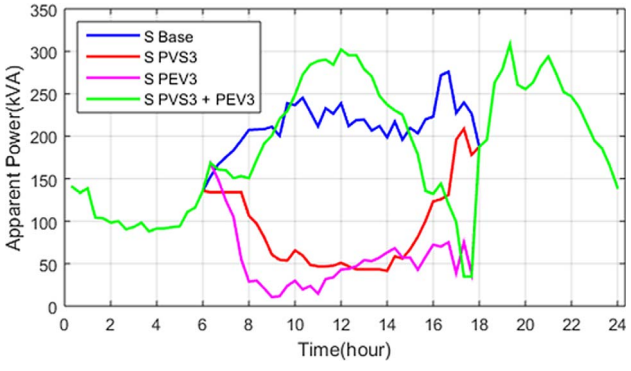

Figure 9. Analysis of day-to-day outlines of domestic load at the transformer 3 during summer.

for all the nodes. The comparison of only PV connection and only PEV connection provides more voltage differences. Compared to PEV, PV provides more voltage difference. Only PV connection at summer, the maximum voltage difference is achieved at node 18 and the voltage difference is 3.2%. Only PEV connection at summer, the maximum voltage difference is achieved at node 18 and the voltage difference is 2.9%. Both PV and PEV connection at summer, the maximum voltage difference is achieved at node 1 and the voltage difference is −0.01%. Analysis of system THD differences in maximum level during summer is shown in Figure 11. Here the nodes and THD differences are present. The THD difference of both the connection of PV and PEV system some value is negative and some are small value in positive for the nodes. The comparison of only PV connection and only PEV connection provides more THD differences. Compared to PEV, PV provides more voltage difference. Only PV connection at summer, the maximum THD difference is achieved at node 18 and the THD difference is 1.15%. Only PEV connection at summer, the maximum THD difference is achieved at node 18 and the THD difference is 1%. Both PV and PEV connection at summer, the maximum THD difference

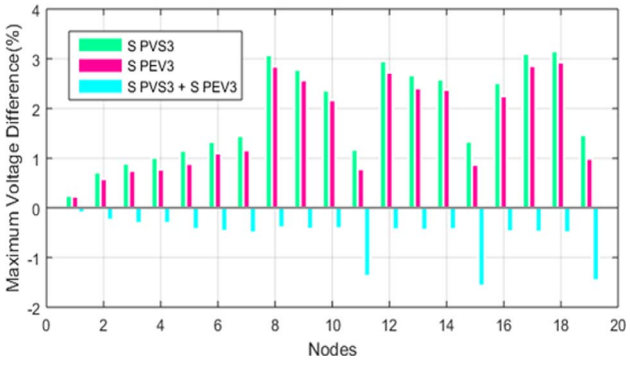

Figure 10. Analysis of system voltage differences in maximum level during summer.

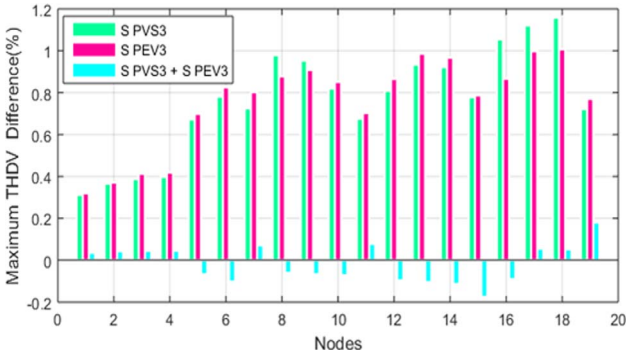

Figure 11. Analysis of system THD differences in maximum level during summer.

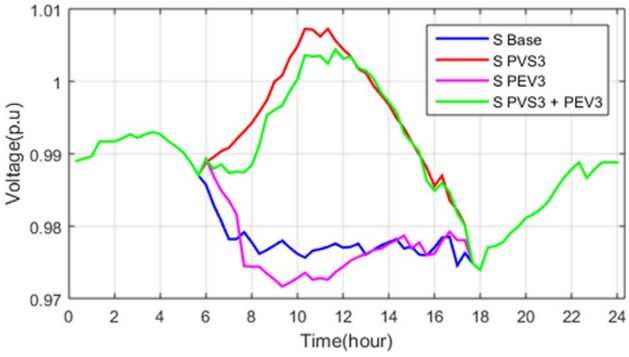

Figure 12. Analysis of daily profiles of phase voltage for summer.

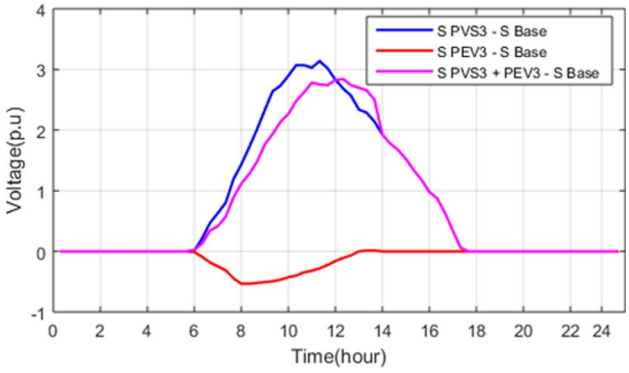

Figure 13. Analysis of daily profiles of phase voltage for summer in relation of base case.

is achieved at node 19 and the THD difference is 0.15%. Analysis of daily profiles of phase voltage for summer is shown in Figure 12. Here considered, the node 18. Consider the time period 6 to 18 h, the maximum voltage at the base cases is 0.985 (p.u), the maximum voltage at the individual connection of PV and PEV becomes 1.006(p.u), 0.989 (p.u) respectively. When both PV and PEV connection, the maximal voltage becomes 1.004(p.u) respectively. Because of the individual impacts in PVS and PEV on the voltage outlines are opposite; their concurrent process reduces the voltage deflection associated with base line. Consequently, depending upon the rate among penetration levels for PV as well as PEV, the voltage is enhanced may lead to a reduction in the PEV load voltage difference. Analysis of daily profiles of phase voltage for summer and winter in relation of base case is displays in Figure 13. Here, the Figure 13 is depicts the voltage variation high with the generation of PV and intensity of PEV connection. The variation of voltage is occurring due to the penetration of PV and PEV. With relation of base case, the PV maximum voltage at summer is 3.1 (p.u), the PEV and both PV and PEV the maximum voltage becomes 0, 2.8 (p.u) respectively. Figure 14 displays the analysis of daily profiles of THD when zero medium voltage grid and PEV harmonic. So the THD percentage at base case is high and the high THD value is obtained at 1.7% at 10 h. THD percentage at only PV connection is around 1.8% at 10 h. THD percentage at only PEV connection is around 1.8% at 10 h. THD percentage at both PV and PEV connection is around 2.3% at 10 h. Figure 14 conclude that at PEV harmonics zero then the combined PV and PEV connection THD is high. Figure 15 displays the analysis of daily profiles of THD when zero medium voltage grid and PEV harmonic and the relation of improper circumstance. Here considered the node 19, and the relation of base case. The PV with comparison of improper circumstance, the maximal variance of THD as of 0.65%, the PEV with comparison of improper circumstance, the maximal variance of THD as of 0.8%, The PV plus PEV with comparison of base case, the maximum variance of THD as of 0.18%. So from the Figure 15, it is concluding that the PV with PEV provides less THD than others. Figure 16 displays the analysis of daily profiles of THD difference when random value of medium voltage grid and PEV harmonic compared to base case. From the Figure 15, it is conclude that both PEV and PV connection provides less THD difference than other case is proved. Figure 17 displays the analysis of daily profiles of THD difference when random value of medium voltage grid and PEV harmonic. From the Figure 17, it is conclude that both PEV and PV connection provides less THD than other case is proved. Figure 18 displays the analysis of daily profiles of THD difference when zero value of medium voltage grid and PEV harmonic compared to base case. From the Figure 18, it is conclude that both PEV and PV connection provides less THD than other case is proved.

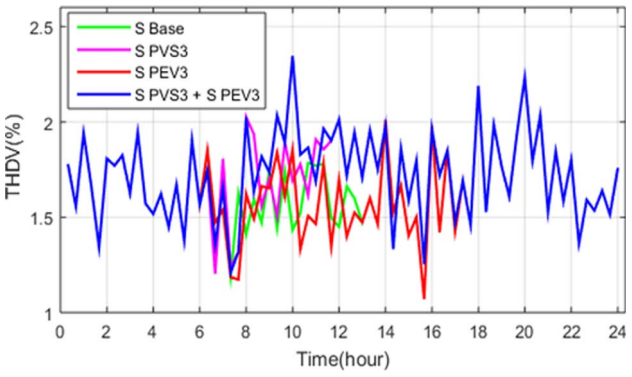

Figure 14. Analysis of daily profiles of THD when zero medium voltage grid and PEV harmonic.

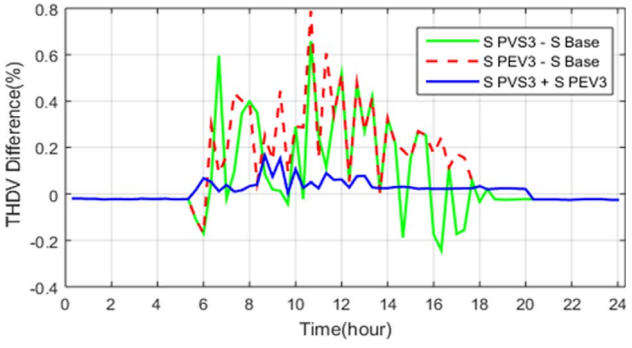

Figure 15. Analysis of daily profiles of THD when zero medium voltage grid and PEV harmonic compared to base case.

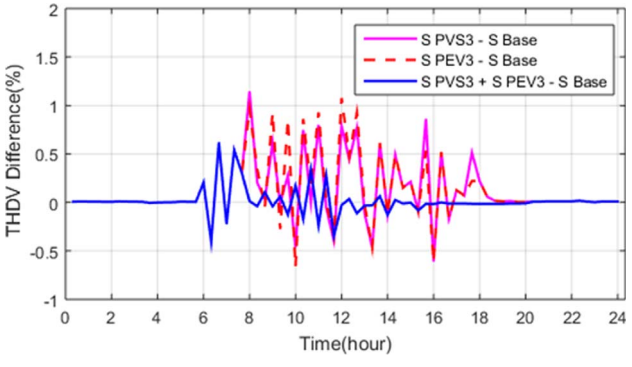

Figure 16. Analysis of daily profiles of THD difference when random value of medium voltage grid and PEV harmonic compared to base case.

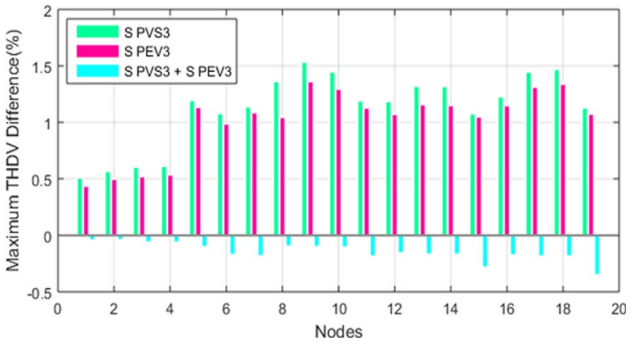

Figure 17. Analysis of daily profiles of THD difference when random value of medium voltage grid and PEV harmonic.

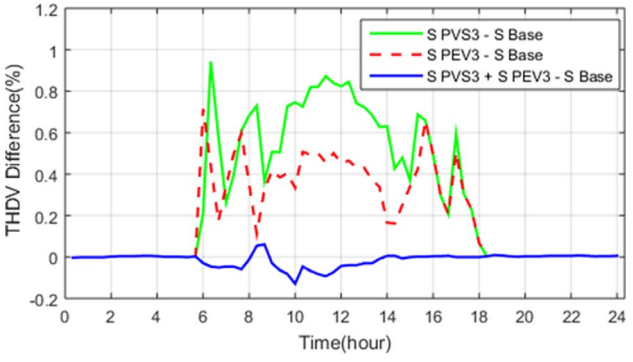

Figure 18. Analysis of daily profiles of THD difference when zero value of medium voltage grid and PEV harmonic compared to base case.

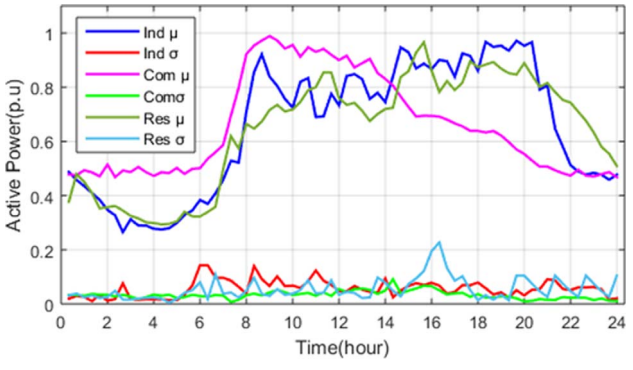

Figure 19. Analysis of statistical parameters of active energy profiles of lumped loads for winter.

Case 2: performance analysis of GRFO-ITSA on winter

Here, the performance of the GRFO-ITSA approach are analyzed in winter season. Figure 19 displays the statistical parameters of active energy profiles of lumped loads for winter. Here present the industrial, commercial, residential load mean and standard deviation. The standard deviation of commercial load active power is varies 0 to 0.1 (p.u) at the time period of 0 to 24 h. Similarly, the standard deviation of industrial load is varies 0 to 0.15 at the time period of 0 to 24 h. The standard deviation of residential load is varies 0 to 0.1 (p.u) at the time period 0 to 15 h, then it increased to 0.22 (p.u) at 16 h. Again the residential mean value of active power is varied as of 0 to 0.1 (p.u). The mean value of industrial load active power is varied up to 0.95 (p.u) and the residential load active power is varied up to 0.95 (p.u) at 15 h. Compared to industrial load active power mean value, the residential load active power mean value is low is presented in Figure 12. The commercial load active power mean value is varied up to 1 (p.u).

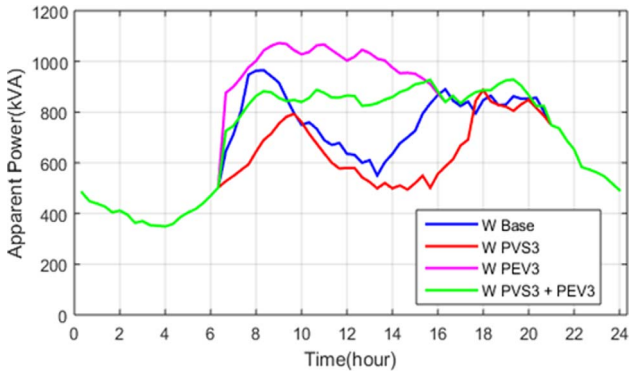

Figure 20. Analysis of day-to-day outlines of the feeder 1 to 2 loads (any type) thru wintertime.

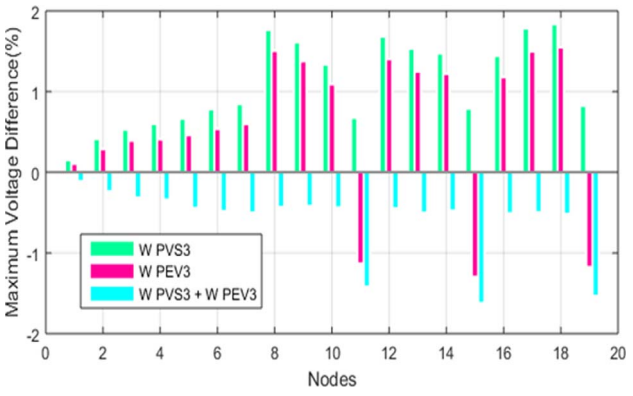

Figure 21. Analysis of system voltage differences in maximum level during winter.

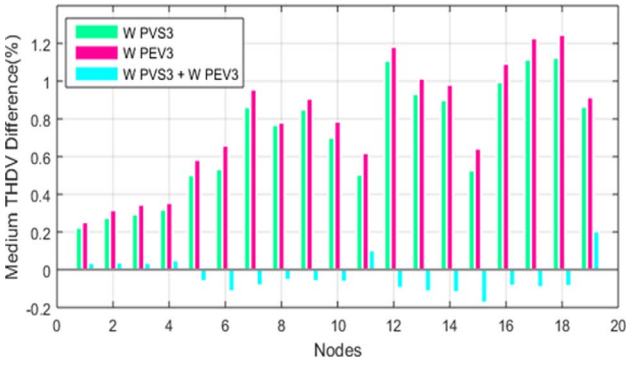

Figure 22. Analysis of system THD differences in maximum level during winter.

By comparing the mean value of manufacturing profitable along domestic load active powers, commercial load active power is high then other two active powers. The active power values are normalized in relative to the maximal active power load. Analysis of daily profile of the feeder 1 to 2 loads (any type) through wintertime is displays in Figure 20. Here, the proposed system is analyzed under four sub cases. S base means the system performance is analyzed at PV system and PEVs are not connected in winter (W). W PVS3 means the system is connected to PV system but not connected to the PEV. W PEV3 means the system is connected to PEV but not connected to the PVs. W PVS3 plus PEV3 means the system is connected to both PVs and PEV. For analyzing the time period of 6 to 18 h, the apparent power at base case is varied up to 950 kVA. Under the connection of PV system, the apparent power is varied up to 800 kVA at 9.5 h. By connecting the PV system, the apparent power is very low. When only connecting the PEV, then the apparent power is varied up to 1050 kVA. It provides high apparent power. When connecting both PEV and PV, the apparent power is varied to 900 kVA. It is higher than the connection of individual PV system. Analysis of system voltage differences in maximum level during winter is shown in Figure 21. Here the nodes and voltage differences are present. The voltage difference of both the connection of PV and PEV system is negative for all the nodes. The comparison of only PV connection and only PEV connection provides more voltage differences. Compared to PEV, PV provides more voltage difference. Only PV connection at summer, the maximum voltage difference is achieved at node 18 and 8 and the voltage difference is 1.8%. Only PEV connection at summer, the maximum voltage difference is achieved at node 18, 8 and the voltage difference is 1.6%. The node 11, 15, 19, only PEV connection provides negative values. Both PV and PEV connection at summer, the maximum voltage difference is achieved at node 1 and the voltage difference is −0.01%.

Analysis of system THD differences in maximum level during winter is shown in Figure 22. Here the nodes and THD differences are present. The THD difference of both the connection of PV and PEV system some value is negative and some are small value in positive for the nodes. The comparison of only PV connection and only PEV connection provides more THD differences. Compared to PEV, PV provides more voltage difference. Only PV connection at summer, the maximum THD difference is achieved at node 17, 18 and the THD difference is 1.21%. Only PEV connection at summer, the maximum THD difference is achieved at node 18 and the THD difference is 1.1%. Both PV and PEV connection at summer, the maximum THD difference is achieved at node 19 and the THD difference is 0.2%.

Case 3: Performance analysis of proposed system in summer and winter

Here, the performance of the GRFO-ITSA approach are analyzed in summer and winter seasons. Figure 23 displays the statistical parameters of active energy profiles for summer and winter. The standard deviation of active power in summer season is varies 0–0.31 (p.u) at 5.8–12 h of time period. At that time it decreased to reaches zero at 16th hour. The mean value of active power in summer is varied from 0 to 0.51 (p.u) at 5 to 10 h. At that time the mean value is decreased to reach zero at 16 h. The standard deviation of active power in winter season is varies 0 to 0.25 (p.u) at 7 to 11 h of time period. At that time it decrease to reaches zero as of 14.5 h. The mean value of active power in winter is varied from 0 to 0.27 (p.u) at

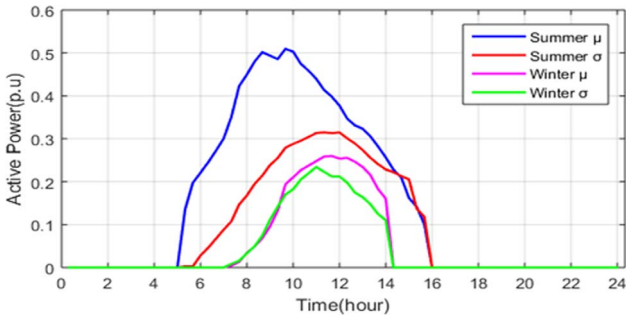

Figure 23. Analysis of statistical parameters of active power outlines in summer as well as winter.

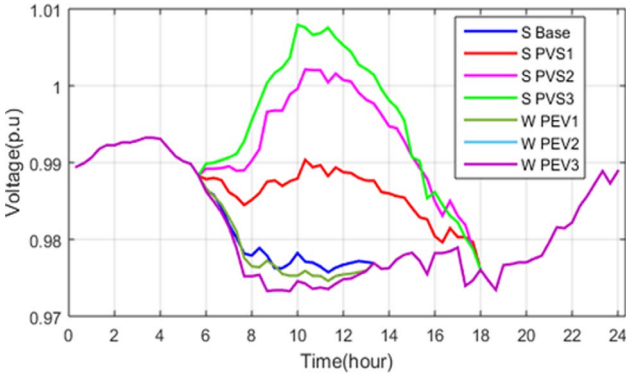

Figure 24. Analysis of daily profiles of voltage in summer as well as winter.

7 to 12 h. Then the mean value is decreased to reach zero at 14.5 h. Compared to winter and summer season statistical characteristic provides the standard deviation, mean value of summer season is high then the winter season.

Analysis of daily profiles of voltage for summer and winter is displays in Figure 24. Here considered varies penetration of PV and PEV. Consider the summer season and the time period 6–16 h then the base case, PV1, PV2, PV3 maximum voltage is becomes 0.978 (p.u), 0.99 (p.u), 0.1003 (p.u), 0.1008 (p.u) respectively. Consider the winter season and the time period 8–12 h then the PEV1, PEV3 maximum voltage is becomes 0.976 (p.u), 0.974 (p.u) respectively.

Comparison of THD of proposed and existing approaches in summer and winter season is shown in Figure 25. The proposed approach THD at summer season is 0.15% and the winter season is 0.2%. The Moth Search Algorithm (MOA) approach THD at summer season is 0.21% and the winter season is 0.28%. The Mayfly Optimization Algorithm (MOA) approach THD at summer season is 0.21% and the winter season is 0.28%. The Moth Search Algorithm (MOA) approach THD at summer season is 0.3% and the winter season is 0.35%. The Grey Wolf Optimizer (GWO) approach THD at summer season is 0.8% and the winter season is 0.9%. From this Figure 24 it is conclude GRFO-ITSA approach THD is less than existing methods is proved.

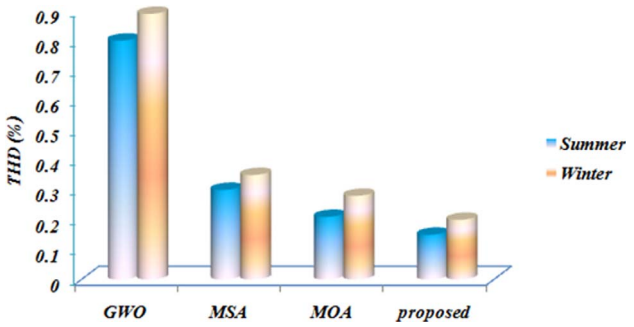

Figure 25. Comparison of THD of proposed and existing approaches in summer and winter season.

7 Conclusion

In this paper proposed a hybrid GRFO-ITSA approach for minimizing the harmonics, voltage deviation and improvement of power quality in the integrated PVs and PEVs clever network system. GRFO determines the reference current for compensating the harmonics and the reactive power of the system. The proposed ITSA approach is utilized to control the flow of load and satisfy the demand of the system. The proposed approach is analyzes the effect of the concurrent joint of the PVs, PEVs on the day-to-day load outline of feeders along transmitters and on the day-to-day voltage as well as THD outlines in the distributing system. Built in proposed approach to modelling of loads, PVs and PEVs are utilized to analyze the connection and disconnection of charge of PEV batteries thru day. The proposed approach is analyzed under two seasons like summer as well as winter. Under this cases, various sub cases are considered to analyze the proposed system. The sub cases are base case, that is the system is not connected in PV and PEV, only PV connection, only, PEV connection and both PV and PEV connection. From this analysis, it is conclude that the proposed approach reduces the harmonics and voltage difference and increase the power quality efficiently.

Data availability

Data sharing is not applicable to this article as no new data were created or analyzed in this study.

Funding

This research did not receive any specific grant from funding agencies in the public, commercial, or not-for-profit sectors.

Ethical approval

This article does not contain any studies with human participants performed by any of the authors.

Conflict of interest

The authors declare that they have no known competing financial interests or personal relationships that could have appeared to influence the work reported in this paper.

References

1 Ellabban O., Abu-Rub H. (2016) Smart grid customers' acceptance and engagement: an overview, *Renew. Sust. Energ. Rev.* **65**, 1285–1298.

2 Levi V., Williamson G., King J., Terzija V. (2020) Development of GB distribution networks with low carbon technologies and smart solutions: scenarios and results, *Int. J. Electr. Power Energy Syst.* **119**, 105832.

3 Sultana B., Mustafa M.W., Sultana U., Bhatti A.R. (2016) Review on reliability improvement and power loss reduction in distribution system *via* network reconfiguration, *Renew. Sust. Energ. Rev.* **66**, 297–310.

4 Wilson D., Yu J., Al-Ashwal N., Heimisson B., Terzija V. (2019) Measuring effective area inertia to determine fast-acting frequency response requirements, *Int. J. Electr. Power Energy Syst.* **113**, 1–8.

5 Jani D.B. (2020) Performance analysis of hybrid cooling systems using artificial neural network, *Glob. J. Energy Technol. Res. Updates* **7**, 12–20.

6 Gielen D., Boshell F., Saygin D., Bazilian M.D., Wagner N., Gorini R. (2019) The role of renewable energy in the global energy transformation, *Energy Strategy Rev.* **24**, 38–50.

7 Javadi A., Hamadi A., Ndtoungou A., Al-Haddad K. (2016) Power quality enhancement of smart households using a multilevel-THSeAF with a PR controller, *IEEE Trans. Smart Grid* **8**, 1, 465–474.

8 Kraiczy M., Stetz T., Braun M. (2017) Parallel operation of transformers with on load tap changer and photovoltaic systems with reactive power control, *IEEE Trans. Smart Grid* **9**, 6, 6419–6428.

9 Shaukat N., Khan B., Ali S.M., Mehmood C.A., Khan J., Farid U., Majid M., Anwar S.M., Jawad M., Ullah Z. (2018) A survey on electric vehicle transportation within smart grid system, *Renew. Sust. Energ. Rev.* **81**, 1329–1349.

10 Verma A.K., Singh B., Shahani D.T., Jain C. (2016) Grid-interfaced solar photovoltaic smart building with bidirectional power flow between grid and electric vehicle with improved power quality, *Electr. Power Compon. Syst.* **44**, 5, 480–494.

11 Tavakoli A., Saha S., Arif M.T., Haque M.E., Mendis N., Oo A.M. (2020) Impacts of grid integration of solar PV and electric vehicle on grid stability, power quality and energy economics: a review, *IET Energy Syst. Integr.* **2**, 3, 243–260.

12 Amjadi Z., Williamson S.S. (2013) Digital control of a bidirectional DC/DC switched capacitor converter for hybrid electric vehicle energy storage system applications, *IEEE Trans. Smart Grid* **5**, 1, 158–166.

13 Naderi Y., Hosseini S.H., Zadeh S.G., Mohammadi-Ivatloo B., Vasquez J.C., Guerrero J.M. (2018) An overview of power quality enhancement techniques applied to distributed generation in electrical distribution networks, *Renew. Sust. Energ. Rev.* **93**, 201–214.

14 Enose N. (2014) Advanced technologies implementation framework for a smart grid, *J. Clean Energy Technol.* **2**, 1, 88–94.

15 Gandoman F.H., Ahmadi A., Sharaf A.M., Siano P., Pou J., Hredzak B., Agelidis V.G. (2018) Review of FACTS technologies and applications for power quality in smart grids with renewable energy systems, *Renew. Sust. Energ. Rev.* **82**, 502–514.

16 Singh S., Singh B., Bhuvaneswari G., Bist V. (2015) Power factor corrected zeta converter based improved power quality switched mode power supply, *IEEE Trans. Ind. Electron.* **62**, 9, 5422–5433.

17 Agarwal R.K., Hussain I., Singh B. (2017) Application of LMS-based NN structure for power quality enhancement in a distribution network under abnormal conditions, *IEEE Trans. Neural Netw. Learn. Syst.* **29**, 5, 1598–1607.

18 Mortezaei A., Simões M.G., Savaghebi M., Guerrero J.M., Al-Durra A. (2016) Cooperative control of multi-master–slave islanded microgrid with power quality enhancement based on conservative power theory, *IEEE Trans. Smart Grid* **9**, 4, 2964–2975.

19 Luo Y., Zhu T., Wan S., Zhang S., Li K. (2016) Optimal charging scheduling for large-scale EV (electric vehicle) deployment based on the interaction of the smart-grid and intelligent-transport systems, *Energy* **97**, 359–368.

20 Mohtashami S., Pudjianto D., Strbac G. (2016) Strategic distribution network planning with smart grid technologies, *IEEE Trans. Smart Grid* **8**, 6, 2656–2664.

21 Balasundar C., Sundarabalan C.K., Sharma J., Srinath N.S., Guerrero J.M. (2021) Design of power quality enhanced sustainable bidirectional electric vehicle charging station in distribution grid, *Sustain. Cities Soc.* **74**, 103242.

22 Gayathri M.N. (2021) A smart bidirectional power interface between smart grid and electric vehicle, in: *Intelligent paradigms for smart grid and renewable energy systems*, Springer, Singapore, pp. 103–137.

23 Brinkel N.B.G., Gerritsma M.K., AlSkaif T.A., Lampropoulos I., van Voorden A.M., Fidder H.A., van Sark W.G.J.H.M. (2020) Impact of rapid PV fluctuations on power quality in the low-voltage grid and mitigation strategies using electric vehicles, *Int. J. Electr. Power Energy Syst.* **118**, 105741.

24 Lara J., Masisi L., Hernandez C., Arjona M.A., Chandra A. (2021) Novel five-level ANPC bidirectional converter for power quality enhancement during G2V/V2G operation of cascaded EV charger, *Energies* **14**, 9, 2650.

25 Irfan M.M., Rangarajan S.S., Collins E.R., Senjyu T. (2021) Enhancing the power quality of the grid interactive solar photovoltaic-electric vehicle system, *World Elect. Veh. J.* **12**, 3, 98.

26 Kavin K.S., Subha Karuvelam P. (2021) PV-based grid interactive PMBLDC electric vehicle with high gain interleaved DC-DC SEPIC Converter, *IETE J. Res.* 1–15.

27 Bajaj M., Singh A.K. (2021) A global power quality index for assessment in distributed energy systems connected to a harmonically polluted network, *Energy Sources A Recovery Util. Environ. Eff.* 1–27.

28 Suganya S., Charles Raja S., Venkatesh P. (2017) Smart management of distinct plug-in hybrid electric vehicle charging stations considering mobility pattern and site characteristics, *Int. J. Energy Res.* **41**, 14, 2268–2281.

29 Li Y., Ni Z., Zhao T., Zhong T., Liu Y., Wu L., Zhao Y. (2020) Supply function game based energy management between electric vehicle charging stations and electricity distribution system considering quality of service, *IEEE Trans. Ind. Appl.* **56**, 5, 5932–5943.

30 Suganya S., Raja S.C., Venkatesh P. (2017) Simultaneous coordination of distinct plug-in Hybrid Electric Vehicle charging stations: A modified Particle Swarm Optimization approach, *Energy* **138**, 92–102.
31 Gampa S.R., Jasthi K., Goli P., Das D., Bansal R.C. (2020) Grasshopper optimization algorithm based two stage fuzzy multiobjectiveapproach for optimum sizing and placement of distributed generations, shunt capacitors and electric vehicle charging stations, *J. Energy Storage* **27**, 101117.
32 Awasthi A., Venkitusamy K., Padmanaban S., Selvamuthukumaran R., Blaabjerg F., Singh A.K. (2017) Optimal planning of electric vehicle charging station at the distribution system using hybrid optimization algorithm, *Energy* **133**, 70–78.
33 Liu J.P., Zhang T.X., Zhu J., Ma T.N. (2018) Allocation optimization of electric vehicle charging station (EVCS) considering with charging satisfaction and distributed renewables integration, *Energy* **164**, 560–574.
34 Mozafar M.R., Moradi M.H., Amini M.H. (2017) A simultaneous approach for optimal allocation of renewable energy sources and electric vehicle charging stations in smart grids based on improved GA-PSO algorithm, *Sustain. Cities Soc.* **32**, 627–637.
35 Pflaum P., Alamir M., Lamoudi M.Y. (2017) Probabilistic energy management strategy for EV charging stations using randomized algorithms, *IEEE Trans. Control Syst. Technol.* **26**, 3, 1099–1106.
36 Shakerighadi B., Anvari-Moghaddam A., Ebrahimzadeh E., Blaabjerg F., Bak C.L. (2018) A hierarchical game theoretical approach for energy management of electric vehicles and charging stations in smart grids, *IEEE Access* **6**, 67223–67234.
37 Zhang H., Hu Z., Xu Z., Song Y. (2016) Evaluation of achievable vehicle-to-grid capacity using aggregate PEV model, *IEEE Trans. Power Syst.* **32**, 1, 784–794.
38 Tushar M.H.K., Zeineddine A.W., Assi C. (2017) Demand-side management by regulating charging and discharging of the EV, ESS, and utilizing renewable energy, *IEEE Trans. Ind. Inform.* **14**, 1, 117–126.
39 Chaudhari K., Ukil A., Kumar K.N., Manandhar U., Kollimalla S.K. (2017) Hybrid optimization for economic deployment of ESS in PV-integrated EV charging stations, *IEEE Trans. Ind. Inform.* **14**, 1, 106–116.
40 Yan Q., Zhang B., Kezunovic M. (2018) Optimized operational cost reduction for an EV charging station integrated with battery energy storage and PV generation, *IEEE Trans. Smart Grid* **10**, 2, 2096–2106.
41 Shojaabadi S., Abapour S., Abapour M., Nahavandi A. (2016) Simultaneous planning of plug-in hybrid electric vehicle charging stations and wind power generation in distribution networks considering uncertainties, *Renew. Energy* **99**, 237–252.
42 Li D., Zouma A., Liao J.T., Yang H.T. (2020) An energy management strategy with renewable energy and energy storage system for a large electric vehicle charging station, *Etransportation* **6**, 100076.
43 Tovilović D.M., Rajaković N.L. (2015) The simultaneous impact of photovoltaic systems and plug-in electric vehicles on the daily load and voltage profiles and the harmonic voltage distortions in urban distribution systems, *Renew. Energy* **76**, 454–464.
44 Rekik M., Krichen L. (2021) Photovoltaic and plug-in electric vehicle for smart grid power quality enhancement, *Arab. J. Sci. Eng.* **46**, 2, 1481–1497.
45 Rekik M., Abdelkafi A., Krichen L. (2015) A micro-grid ensuring multi-objective control strategy of a power electrical system for quality improvement, *Energy* **88**, 351–363.
46 Jaber A.S., Abdulbari H.A., Shalash N.A., Abdalla A.N. (2020) Garra Rufa-inspired optimization technique, *Int. J. Intell. Syst.* **35**, 11, 1831–1856.
47 Fetouh T., Elsayed A.M. (2020) Optimal control and operation of fully automated distribution networks using improved tunicate swarm intelligent algorithm, *IEEE Access* **8**, 129689–129708.